Electronic Energy Transfer in Multichromophoric Arrays. A Sequential and Superexchange Dynamics Study

Edwin K. L. Yeow, David J. Haines, and Kenneth P. Ghiggino*

Photophysics Laboratory, School of Chemistry, The University of Melbourne, Parkville, Victoria 3052, Australia

Michael N. Paddon-Row

School of Chemistry, The University of New South Wales, Sydney 2052, Australia

Received: April 1, 1999

The dynamics of electronic energy transfer (EET) from a photoexcited donor to an acceptor connected by an intermediate bridge is investigated using the Haken, Strobl, and Reineker stochastic Liouville equations (HSR). The effects of the system−bath interaction on both the superexchange and sequential energy transfer mechanisms via the bridge are discussed and subsequently used to explain the role of the bridge in mediating EET. We examine the mechanisms of EET in a rigidly linked naphthalene dimer where the chromophores are separated by six σ bonds (DN-6). Experimental studies of EET using fluorescence anisotropy measurements indicate that the superexchange mechanism dominates in DN-6.

1. Introduction

Electronic energy transfer (EET) is a fundamentally important process in chemistry, biology, and physics. In particular, EET has been the topic of active research in studies of photon collection in photosynthetic systems,[1,2] in polymer photophysics,[3,4] for determining proximity relations in proteins,[5] and investigating energy migration in Langmuir−Blodgett films.[6] Understanding the mechanisms by which energy transfer occurs in such multichromophoric arrays poses a major challenge for photochemists and is important for designing useful photomolecular systems.

There have been many experimental and theoretical investigations on EET between molecules in the condensed phase. Förster was the first to derive an equation for the rate of singlet−singlet EET for molecules having broad spectra in a condensed medium[7]

$$k = \left(\frac{1}{\tau_D}\right)\left(\frac{R_o}{R}\right)^6 \tag{1a}$$

where τ_D is the fluorescence lifetime of the donor D in the absence of the acceptor A, R is the distance between D and A, and R_o is the critical distance where the transfer probability equals the emission probability. R_o is defined by

$$R_o^{\,6} = \frac{9000(\ln 10)\kappa^2\phi_D J(\tilde{\nu})}{128\pi^5 N\eta^4} \tag{1b}$$

where ϕ_D is the fluorescence quantum yield of the donor, N is Avogadro's number, η is the refractive index of the solvent, κ^2 is the orientation factor, and $J(\tilde{\nu})$ is the spectral overlap integral of the emission of D with the absorption of A.

Equations 1a and 1b can be derived quantum mechanically via Fermi's golden rule

$$k = \frac{2\pi}{\hbar}|V|^2\delta(E_D - E_A) \tag{2}$$

where only the Coulombic dipole−dipole interaction is considered and the vibrational overlap factor is thus expressed in terms of experimentally obtainable absorption and emission spectra. In general, the effective electronic coupling matrix element, V, is best written as a sum of a number of electronic coupling terms (u)

$$V = u^{\text{Coulombic}} + u^{\text{short-range}} + u^{\text{relay}} \tag{3}$$

where $u^{\text{Coulombic}} = u^{\text{dipole-dipole}} + u^{\text{higher multipole}}$ and $u^{\text{short-range}} = u^{\text{penetration}} + u^{\text{Dexter Exchange}} + u^{\text{tc}}$. The through-configuration term, u^{tc}, arises from the configuration interaction between the locally excited states (A*B and AB*) with the charge-separated states (A^-B^+ and A^+B^-) and has been shown to be the most important term in $u^{\text{short-range}}$.[8−10] The other terms have previously been defined by Scholes and Ghiggino.[11] In this work we are most interested in the relayed interaction term u^{relay}, which involves the transfer of energy from the donor to the acceptor via intermediate moieties or connecting bridges. When there is an insignificant population of energy on the bridge, the process is often called the superexchange mechanism. An example is the "through-bond interaction" (u^{tb}), where the σ bonds connecting the two chromophores act as the "relay units".[12] McConnell's perturbative model best illustrates the dependence of u^{tb} on the energy gap between the donor/acceptor and the bridge ω, the coupling between two adjacent bridge subunits v, the coupling between the donor/acceptor and the adjacent bridge V, and the number of bridge subunits n:[13]

$$u^{\text{tb}} = \left(\frac{V^2}{-\omega}\right)\left(\frac{v}{-\omega}\right)^{n-1} \tag{4}$$

Recently there have been a number of investigations on the interplay between the superexchange and sequential (i.e. local-

* Corresponding author. E-mail: k.ghiggino@chemistry.unimelb.edu.au.

10.1021/jp991113b CCC: $18.00
Published on Web 08/04/1999

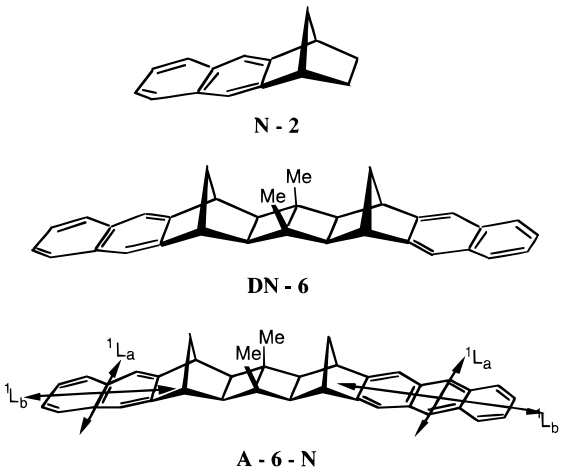

Figure 1. Structures of the rigidly linked bichromophoric systems DN-6 and A-6-N along with the model compound N-2.

ization of electrons onto the relay units) electron-transfer mechanisms via the bridge.[14−18] These competing processes have been used to explain the anomalous distance dependence of long-range electron transfer in DNA. Friesner et al.[17] and Ratner et al.[18] have used the multilevel Redfield equations and the phenomenological Bloch equations respectively to highlight the importance of coherence dephasing by the bath to induce the sequential mechanism. Under the existing conditions of "modest" donor−bridge energy gap and large dephasing, the incoherent sequential mechanism arises even though the bridge population is small. This mechanism has been shown to dominate the superexchange mechanism when the bridge length is increased considerably.[17,18]

In this paper we investigate the same problem in the context of electronic energy transfer. The ultimate goal is then to offer a more concise explanation for the EET dynamics occurring in a polynorbornane-bridged naphthalene dimer, DN-6 (see Figure 1), using either or both of the superexchange and sequential mechanisms. We have previously reported the preliminary results of EET rates in DN-6 which indicate the need to invoke other mechanisms apart from Förster theory.[19,20] We present here more detailed fluorescence anisotropy decay measurements which provide results of energy transfer rates to compare with theory. To incorporate the system−bath interaction, we have chosen to work with the most accessible set of density matrix equations derived by Haken, Strobl, and Reineker (HSR).[21,22] The HSR equations have commonly been used to elucidate the coherent and incoherent nature of energy transfer in molecular crystals[23] and more recently in bacteriochlorophyll systems.[24,25] In this work, we find that the HSR theory also provides a means of studying the role of the bridge in mediating energy transfer. It is shown that, depending on the donor−bridge energy gap and the extent of the system-bath interaction, the bridge may activate both the superexchange and sequential mechanisms to differing extents.

This paper is organized as follows: The experimental procedures are outlined in section 2. The HSR theory and the computational method are given in section 3. In section 4, we use the HSR equations to examine the EET dynamics in resonant and nonresonant two-site systems. The theory is then extended to a three-site system inclusive of a pair of resonant molecules connected by a bridge of higher energy. The competition between the superexchange and sequential mechanisms is demonstrated. In section 5, we apply the concepts developed to the DN-6 molecule. The implications of the work for more extended polymeric systems and the conclusion are presented in section 6.

2. Experimental Section

The synthesis of DN-6 and the model chromophore N-2 (Figure 1) have been described elsewhere.[26] The optimized geometry for DN-6 was determined by the MNDO method with a C_{2v} symmetry constraint resulting in the center-to-center separation and edge-to-edge separation of the chromophores of 11.26 and 7.56 Å, respectively, as defined in ref 20.

Solutions of DN-6 were prepared in 2-methyltetrahydrofuran (MTHF) to absorbances of less than 0.2 at 317 nm for both steady-state and time-resolved fluorescence measurements. The samples were thoroughly degassed by repeated freeze−pump−thaw cycles to remove any dissolved gases before being cooled to a glassy state and maintained at 77 K using a variable temperature liquid nitrogen cryostat (Oxford Instruments Optistat). This is necessary to eliminate any fluorescence depolarization caused by molecular rotation. Steady-state fluorescence measurements were recorded on a Hitachi F-4500 fluorescence spectrophotometer.

The time-resolved fluorescence lifetimes and anisotropy were measured using the time-correlated single photon counting method. The excitation source is a synchronously pumped and cavity dumped dye laser (Spectra Physics 3500) which provided excitation pulses of ca. 5 ps fwhm at a repetition rate of 4 MHz. The output of the DCM dye used was frequency doubled in a KDP crystal, and the samples were excited into the first absorption band of DN-6 (316 nm to 318 nm). Fluorescence lifetime measurements were recorded by observing the emission through a polarizer set at the magic angle (54.7°) relative to the vertically polarized excitation light. The parallel ($I_{||}(t)$) and perpendicular ($I_{\perp}(t)$) decay profiles were measured by monitoring fluorescence through a polarizer oriented parallel and perpendicular to the vertically polarized excitation beam. All measurements were recorded at an emission wavelength of 334 nm. The decay data were collected over 512 channels on a multichannel analyzer and were analyzed using the nonlinear least squares iterative reconvolution procedures based on the Marquardt algorithm.[27] Fluorescence anisotropy profiles were generated using the following equation

$$r(t) = \frac{I_{||}(t) - I_{\perp}(t)}{I_{||}(t) + 2I_{\perp}(t)} \tag{5}$$

Since there is no molecular rotation in the rigid low temperature glass, any time-dependent change in fluorescence anisotropy should arise only from energy transfer between the two chromophores. The model compound N-2 exhibited no decay of the fluorescence anisotropy under the experimental conditions in an MTHF glass at 77 K.[19]

3. Theory

The total Hamiltonian for a system interacting with a bath can be written as

$$H = H_0 + H_1 \tag{6}$$

where H_0 and H_1 are the system Hamiltonian and the system−bath Hamiltonian respectively. For a system consisting of an energy donor D and an acceptor A connected by N bridges, H_0 is given by

$$H_0 = \epsilon_D b_D^+ b_D^- + \epsilon_A b_A^+ b_A^- + \sum_{i=1}^{N} \epsilon_i b_i^+ b_i^- + \sum_{i,j=1}^{N} V_{i,j} b_i^+ b_j^- + V_{D,A} b_D^+ b_A^- + V_{A,D} b_A^+ b_D^- \quad (7)$$

where b_i^+ (b_i^-) are the excitation creation (annihilation) operator on site i, ϵ_i is the energy at site i, and $V_{i,j}$ is the electronic interaction energy between neighboring sites i and j.

The reduced density matrix of the system and the bath satisfies the Liouville equation ($\hbar = 1$)[28]

$$\frac{d\rho}{dt} = -i[H_0,\rho] - i[H_1,\rho] \quad (8)$$

The first term in eq 8 describes the coherent motion of the exciton, whereas the second term describes the incoherent dynamics arising from bath fluctuations. The HSR equations are easily derived when H_1 is treated as a Gaussian stochastic process:[21−23]

$$\frac{d\rho_{nn'}}{dt} = -i[H_0,\rho] - \delta_{nn'} \sum_{\nu} 2\gamma_{|n-\nu|}(\rho_{nn} - \rho_{\nu\nu}) - (1 - \delta_{nn'})(\Gamma\rho_{nn'} - 2\bar{\gamma}_{n-n'}\rho_{n'n}) \quad (9)$$

where $\gamma_{nn'}$, $\bar{\gamma}_{n-n'}$ and $\Gamma = 2\sum_\nu \gamma_{|n-\nu|}$ are the HSR parameters defined on the microscopic level.

To simplify our calculations, we have used approximations previously employed by other workers.[23] In this case, the least physical part of eq 9, $\bar{\gamma}_{n-n'}$, is excluded since $\gamma_{nn'}\gamma_{n'n} \geq |\gamma_{n-n'}|^2$ and its inclusion does not yield any novel physical behavior.[22,23,25] Furthermore, the nonlocal fluctuation effects on the interaction energy V and the dissipation of energy via fluorescence are ignored in section 4. These approximations hold when individual $\gamma_{|n-\nu|}$ is much smaller than Γ and the lifetime of the system is large. A comparison of the HSR with the phenomenological Bloch equation reveals that Γ is analogous to the transverse decay rate, $1/T_2$, and is well-approximated by the spectral bandwidth of the molecule.[22] The effects of nonlocal fluctuations and the fluorescence lifetime will be considered only during the analysis of DN-6, where for the latter, the terms introduced by Rahman et al.[29] that correctly explain the effects of fluorescence and radiative decay are applied in section 5. Thus for a two-site system, the following extra terms appear in eq 9:

$$\frac{d\rho_{11}}{dt} = ... - \frac{\rho_{11}}{\tau} - \left(\frac{\cos\theta}{2\tau_o}\right)(\rho_{12} + \rho_{21}) \quad (10a)$$

$$\frac{d\rho_{22}}{dt} = ... - \frac{\rho_{22}}{\tau} - \left(\frac{\cos\theta}{2\tau_o}\right)(\rho_{12} + \rho_{21}) \quad (10b)$$

$$\frac{d\rho_{12}}{dt} = ... - \frac{\rho_{12}}{\tau} - \left(\frac{\cos\theta}{2\tau_o}\right)(\rho_{11} + \rho_{22}) \quad (10c)$$

$$\frac{d\rho_{21}}{dt} = ... - \frac{\rho_{21}}{\tau} - \left(\frac{\cos\theta}{2\tau_o}\right)(\rho_{22} + \rho_{11}) \quad (10d)$$

where $1/\tau$ and $1/\tau_o$ are the fluorescence and radiative decay rates, respectively, and θ is the angle between the transition dipole moments.

The formal solution of eq 9 is given by

$$\rho_{nn'} = G(t)\,\rho(0) \quad (11)$$

The diagonal elements of the density matrix, ρ_{nn}, describe the probability of finding the excitation at site n, while the off-diagonal elements, $\rho_{nn'}$, describe the phase relations between sites n and n'. $G(t)$ is Green's function, which is usually expressed in terms of the eigenvalues (λ) and eigenvectors (M) of eq 9

$$G(t) = M \exp(\lambda t) M^{-1} \quad (12)$$

and $\rho(0)$ is the initial distribution of energy. Since we are interested in the dynamics of energy transfer, the initial excitation is assumed to be localized on the donor site. The eigenvalues and eigenvectors used in this work were computed using the EISPACK[30] matrix eigensystem routines and the inverse matrix, M^{-1}, was obtained using the LINPACK[31] subroutines. All computations were carried out on a Cray J916 computer.

The decay rate used in this work is defined as the average population decay rate, S^{-1}, where S is given as

$$S = \int_0^\infty dt\, \bar{\rho}_{11}(t) \quad (13)$$

and $\bar{\rho}(t) = \rho(t) - \rho(\infty)$, $\bar{\rho}(0) = 1$. The simulated time-resolved anisotropy for a two-site system will be described by

$$r(t) = \frac{\rho_{11}(t) r_1 + \rho_{22}(t) r_2}{\rho_{11}(t) + \rho_{22}(t)} \quad (14)$$

where r_1 and r_2 are the intrinsic fluorescence anisotropies of the donor and acceptor respectively (i.e. the anisotropy in the absence of energy transfer).

4. Model Studies

4.1. Resonant Two-Site System. The rate of energy transfer can be studied by examining the smallest real value of λ (see eq 12). For a resonant two-site system, we can thus obtain λ by solving the cubic equation:

$$\lambda^3 + 2\Gamma\lambda^2 + (4V^2 + \Gamma^2)\lambda + 4V^2\Gamma = 0 \quad (15)$$

to give

$$\lambda = \frac{-\Gamma + \sqrt{\Gamma^2 - 16V^2}}{2} \quad (16)$$

The square root term in eq 16 can be expanded via Taylor's series to give

$$(\Gamma^2 - 16V^2)^{1/2} = \Gamma - \frac{16V^2}{2\Gamma} + ... \quad (17)$$

From eqs 16 and 17, we obtain for the underdamped (weak bath-fluctuation Γ) and overdamped (strong Γ) regimes, respectively,

$$\lambda = \begin{cases} -\dfrac{\Gamma}{2} & (\Gamma < 4V) \\ -\dfrac{4V^2}{\Gamma} & (\Gamma \gg 4V) \end{cases} \quad (18a,18b)$$

The overdamped λ term is simply the golden rule expression which corresponds to the very weak coupling limit of Förster. Figure 2a,b shows the time evolution of the donor population for a dimer system with coupling energy $V = 50$ cm^{-1} (9.4 ps^{-1}) and over a range of different bath-fluctuation energies Γ.

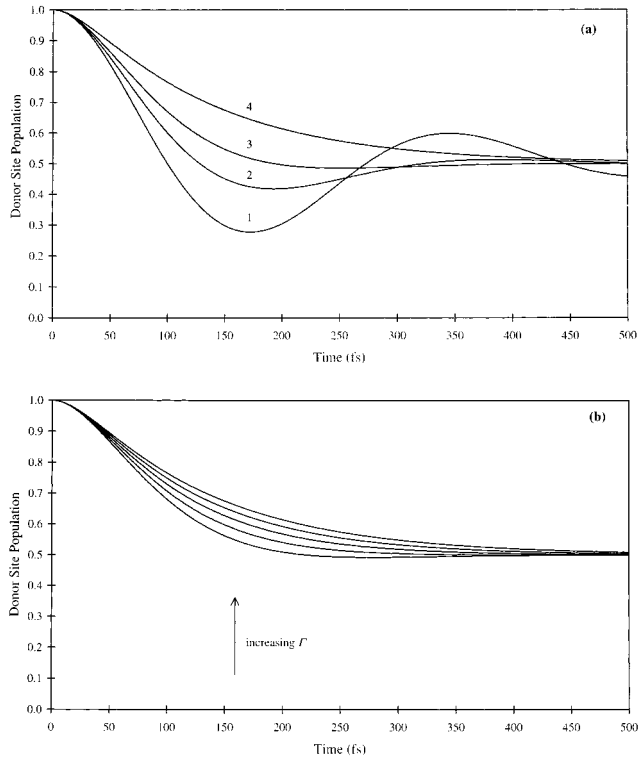

Figure 2. Time evolution of the donor site population for a resonant two-site system at different system−bath fluctuation energies. For panel a, curves 1, 2, 3, and 4 correspond to $\Gamma = 50$, 100, 150, and 266 cm^{-1}. For panel b, the increasing Γ values are from 30 ps^{-1} (160 cm^{-1}) to 50 ps^{-1} (266 cm^{-1}) inclusive and in increment of 5 ps^{-1}. $V = 50$ cm^{-1} for all three cases.

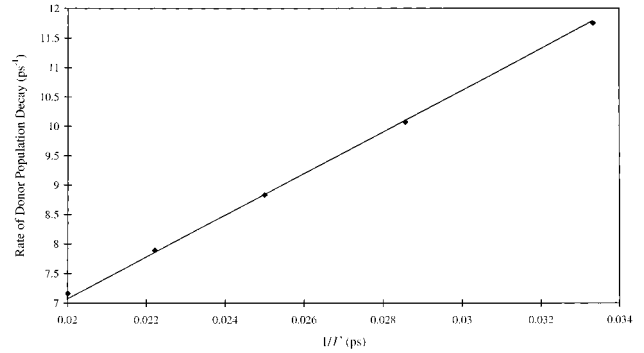

Figure 3. Average decay rate of the donor population against Γ^{-1} for the systems described in Figure 2b. The gradient of the line is 353.66 ps^{-2}.

When $\Gamma = 50$ cm^{-1} the population decay profile exhibits a damped oscillatory motion. This oscillation in motion becomes less apparent when Γ is increased and is totally absent in the overdamped region as expected. Behavior of the population decay rate near the critically damped value (e.g. in the case for $\Gamma = nV$ where $n = 3$, 4, or 5) is worth attention. To examine this region more closely, the average decay rates for the donor population in Figure 2b are obtained and plotted against the reciprocal of their corresponding bath fluctuation. The result is a straight line with a gradient of 354 ps^{-2} (Figure 3). This is compared to the overdamped regime where the same treatment is applied to the time-resolved donor populations for several values of $\Gamma \gg 2V$ (Figure 4). A straight line of a similar gradient is obtained. This suggests that at the region close to the critically damped value, the EET dynamics can be described by the golden rule equation (eq 18b) with $V^2 = 88.5$ ps^{-2} for our model system.

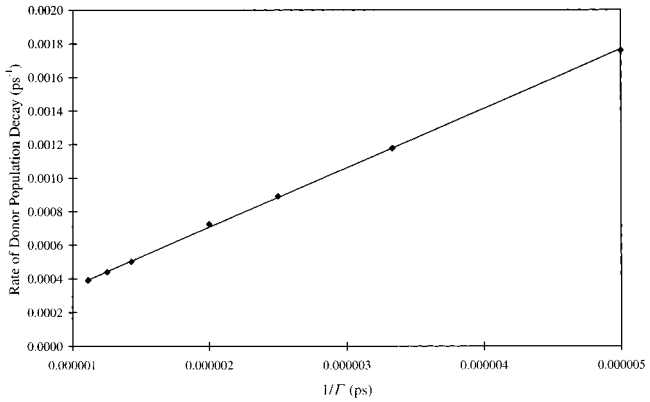

Figure 4. Average decay rate of the donor population against Γ^{-1} for systems with $\Gamma \gg 2V$. Gradient of the line is 353.75 ps^{-2}.

4.2. Nonresonant Two-Site System. We examine the Green's function elements in eq 11 using Leegwater's formalism.[24] By taking the Laplace transform we find

$$\rho(z) = G(z)\rho(t = 0) \tag{19}$$

such that

$$G(z) = \frac{1}{z - iL + \Gamma - \hat{\Gamma}} \tag{20}$$

where $\hat{\Gamma}|i\rangle\langle j| = \Gamma\delta_{ij}|i\rangle\langle j|$.

In terms of the T matrix, $G(z)$ can also be expressed as

$$G(z) = G_0(z) + G_0(z)T(z)G_0(z) \tag{21}$$

where $T(z) = \hat{\Gamma}/[1 - G_0(z)\hat{\Gamma}]$. In the limit when $\Gamma \gg V$,

$$G_0 = \frac{1}{\Gamma} - \frac{1}{\Gamma^2}[H,...] + \frac{1}{\Gamma^3}[H,[H,...]] - ... \tag{22}$$

which takes the form

$$G_0 = \frac{1}{\Gamma} - \frac{2V^2}{\Gamma^3} + \frac{2V^2\omega^2}{\Gamma^5} - \frac{2V^2\omega^4}{\Gamma^7} + ... \tag{23}$$

We can examine two limiting regimes. In the limit of $\Gamma \gg \omega$, we note that

$$[1 - G_0(z)\hat{\Gamma}] = \frac{1}{\Gamma}\left(\frac{2V^2}{\Gamma}\right) \tag{24}$$

and ignoring the $1/\Gamma$ term in $G(z{=}0)$, we obtain $G(z{=}0) = (2V^2/\Gamma)^{-1}$, which is similar to Förster's theory.[24] Therefore when the bath fluctuation is much greater than the energy gap, the site energy of the acceptor becomes isoenergetic with the donor and the acceptor is populated by a single hop. On the other hand when $\Gamma \ll \omega$, we have the following expansion:

$$[1 - G_0(z)\hat{\Gamma}] = \frac{2V^2}{\Gamma^2}\left(1 - \frac{\omega^2}{\Gamma^2} + \frac{\omega^4}{\Gamma^4} - ...\right) \tag{25}$$

Using the expression

$$\left(1 - \frac{\omega^2}{\Gamma^2} + \frac{\omega^4}{\Gamma^4} - ...\right) = \left(1 + \frac{\omega^2}{\Gamma^2}\right)^{-1} \tag{26}$$

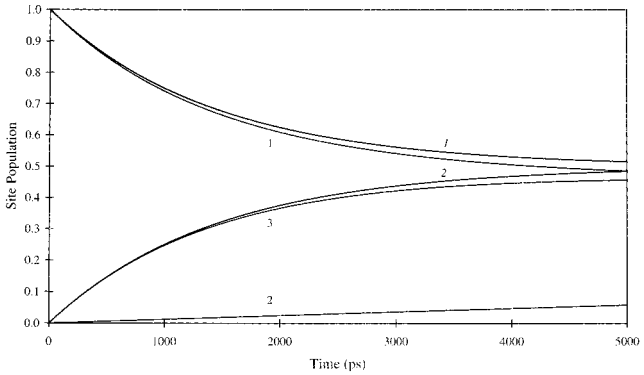

Figure 5. Time dependent site population for a three-site system (1 = donor, 2 = bridge, and 3 = acceptor) with $V = 50$ cm^{-1} (9.4 ps^{-1}), $\omega = 26600$ cm^{-1}, and $\Gamma = 10$ cm^{-1} and for the corresponding two-site McConnell system (*1* = donor and *2* = acceptor).

we can recast eq 25 into eq 27,

$$[1 - G_0(z)\hat{\Gamma}] = \frac{2V^2}{\Gamma^2}\left(1 + \frac{\omega^2}{\Gamma^2}\right)^{-1} \tag{27}$$

which reduces to eq 28 when $\Gamma \ll \omega$

$$[1 - G_0(z)\hat{\Gamma}] = \frac{1}{\Gamma}\left(\frac{2V^2\Gamma}{\omega^2}\right) \tag{28}$$

The EET rate is now proportional to the product of the square of the coupling and the bath fluctuation $V^2\Gamma$ and inversely proportional to the energy gap squared ω^2. The above results complement those of Friesner and co-workers, who looked at the two-level systems using the Redfield equations.[17]

4.3. Three-Site System. In this section, the EET dynamics for a three-site system consisting of energetically degenerate donor and acceptor groups connected via a higher energy bridge is investigated. Figure 5 displays the time evolution of the site population for the three-site system with $V = 50$ cm^{-1}, $\Gamma = 10$ cm^{-1} (1.8 ps^{-1}), and the energy gap between the donor(acceptor) and the bridge $\omega = 26\,600$ cm^{-1} (5000 ps^{-1}). In this case we have ignored any possible through-space interaction between the donor and acceptor. Also displayed in Figure 5 is the site population profiles for a two-site system with a coupling of 0.094 cm^{-1} (0.0177 ps^{-1}) calculated using McConnell's eq 4 and the parameters used for the three-site system. We note that for the three-site system, the population decay of the donor and the population rise of the acceptor agree quite well with the calculated McConnell's coupling. The slightly faster decrease in the donor population is attributed to the very small bridge population. Figure 6 shows the same profile for a three-site system with various values of donor/acceptor−bridge coupling. Both the donor population decay and the acceptor population grow-in with time increase with larger coupling, while the bridge population change is insignificant. This suggests that the role of the connecting bridge is to effect orbital overlap between the distant donor and acceptor molecules, thus facilitating energy transfer by virtual occupation of the bridge. This is consistent with the superexchange mechanism.

When the energy gap is reduced and/or the bath fluctuation is increased, interesting features of EET dynamics are observed. Figure 7 shows the time-dependent site population for a three-site system with $\Gamma = 100$ cm^{-1} (18.8 ps^{-1}) and $\omega = 5320$ cm^{-1} (1000 ps^{-1}) together with the corresponding two-site system with McConnell's coupling. There is now a significant population of excitation onto the bridge such that the equilibrium

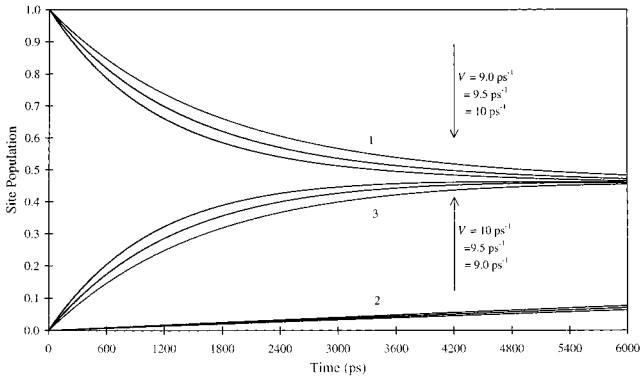

Figure 6. Time dependent site population for a three-site system with $\Gamma = 10$ cm^{-1}, $\omega = 26600$ cm^{-1}, and $V = 9$ ps^{-1}, 9.5 ps^{-1} and 10 ps^{-1}.

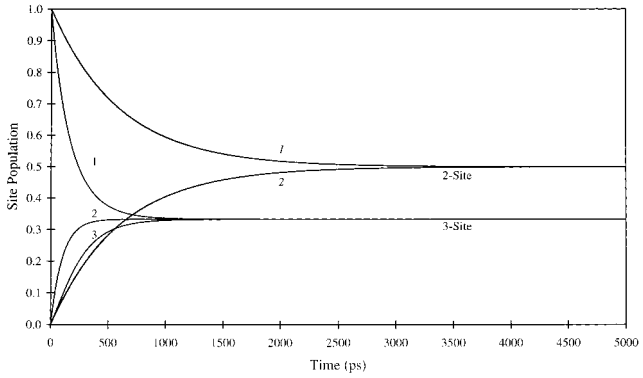

Figure 7. Time dependent site population for a three-site system (1 = donor, 2 = bridge, and 3 = acceptor) with $V = 50$ cm^{-1}, $\omega = 5320$ cm^{-1}, and $\Gamma = 100$ cm^{-1} and for the corresponding two-site McConnell system (*1* = donor and *2* = acceptor).

populations on all three molecules are equal. Furthermore the time taken to reach an equilibrium population is faster than predicted by McConnell's coupling. This is due to the existence of another possible EET channel apart from the superexchange mechanism. Because of the lower energy gap and the higher bath fluctuation, the energy is now transported from the donor to the acceptor by sequential energy hops via the bridge. This is evident not only from the significant population of the bridge but also from the fact that the acceptor becomes populated only after a population has appeared on the bridge.

The salient point to note from the above result is the need for a relatively high bath-fluctuation and a modest enough energy gap to activate the sequential EET mechanism. In the limit of eq 28, it is not difficult to populate the bridge by electronic coupling when either Γ is increased and/or ω is reduced. An analytical expression for the steady-state electron-transfer rate in a similar three-site system derived by Ratner and co-workers[18] using phenomenological equations shows similar trends. Their rate is composed of a McConnell part, which is bath-fluctuation independent, and a dephasing part, which becomes more important with increasing bath-fluctuation energy.

5. EET in a Model Bichromophoric System, DN-6

5.1. EET Dynamics from Fluorescence Anisotropy Decay Profiles. The Förster energy transfer rate for DN-6 was calculated using a slightly modified form of eq 1,

$$k_{\mathrm{EET}}^{\mathrm{dp-dp}} = \frac{V^2 S}{c\hbar^2} \tag{29}$$

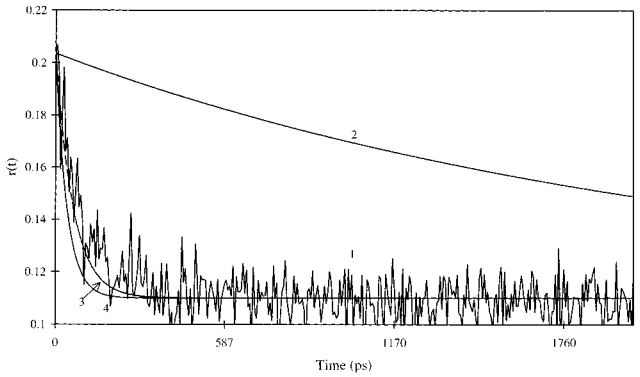

Figure 8. Experimental (1) and simulated (2, 3, and 4) time-resolved fluorescence anisotropy decay profiles for DN-6 in MTHF at 77 K. Simulated curves 2 and 3 are obtained from the PME model with Coulombic transfer rate of $k = 0.22$ ns^{-1} and effective transfer rate of $k = 8.0$ ns^{-1}, respectively. Curve 4 is obtained from the HSR model with the parameters given in the text.

where the dipole−dipole interaction energy between D and A is given by $V = \kappa\mu_D\mu_A/4\pi\epsilon_o\eta^2R^3$, and $\mu_{D(A)}$ is the dipole moment of D(A). S defines the *normalized* spectral overlap such that when both the absorption and emission spectra are represented by Gaussian distributions,

$$S = \frac{1}{\sqrt{2\pi}\sigma_{DA}} \exp\left(-\frac{\Delta^2}{2\sigma_{DA}{}^2}\right) \tag{30}$$

where Δ is the Stokes shift and $\sigma_{DA}{}^2 = 2\sigma^2$, σ being the standard deviation of the molecular bandwidth. The calculated rate for DN-6 is 0.22 ns^{-1} when $\kappa^2 = 2.5$, $\mu_{D(A)} = 1.2 \times 10^{-30}$ Cm, $R = 11.6$ Å, $\sigma = 148$ cm^{-1}, and $\Delta = 109$ cm^{-1}. Both the Pauli Master equation (PME) simulated ($k = 0.22$ ns^{-1}) and experimental fluorescence anisotropy profiles are shown in Figure 8. It is clear that the observed rate of depolarization is much faster than predicted assuming a Förster dipole−dipole mechanism alone. This suggests that other energy transfer mechanisms are operative. In particular we have suggested that the electronic coupling between the two chromophores in this molecule can be enhanced over direct through-space Coulumbic and orbital-overlap-dependent interactions by superexchange involving the much higher energy polynorbonane bridge.[19] In the following we shall attempt to quantify this enhancement.

An approximate value for the effective interaction between the chromophores is obtained from the CNDO/S calculations performed by Clayton and co-workers.[32] Here an estimate for the singlet−singlet EET direct transfer interaction is simply taken to be half the exciton splitting of the S_0-S_1 absorption spectrum obtained from the CNDO/S calculations.[32] For DN-6 we find that $V = 4$ cm^{-1} or 2.02 cm^{-1} when the correction factor n^{-2} is taken into account.[33] The radiative decay rate is estimated from

$$k_{rad} = \frac{\phi_D}{\tau_f} \tag{31}$$

where for the model chromophore N-2 (Figure 1) the experimentally determined values of τ_f and ϕ_D are 72 ns and 0.251, respectively. The HSR anisotropy profile generated from the above parameters is shown to be in better agreement with the experimental results (see Figure 8). The semiempirical approximation thus seems to predict the electronic coupling fairly accurately. By applying eq 3 and ignoring both higher multipole Coulumbic interactions and through-configuration interaction,

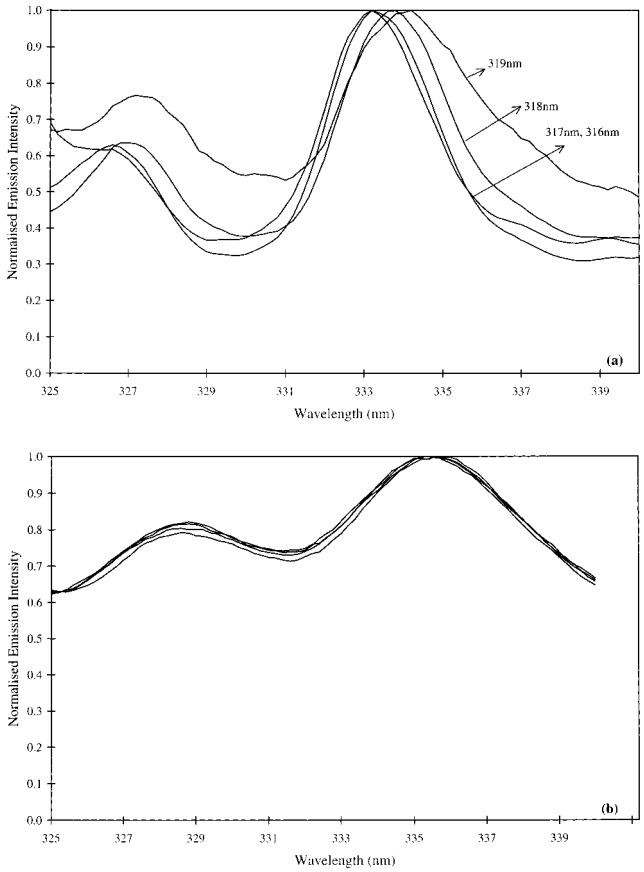

Figure 9. Emission spectra of DN-6 in MTHF at (a) 77 K and (b) room-temperature recorded at several excitation wavelengths.

we can estimate the superexchange contribution to the total interaction to be $u^{tb} = 1.7$ cm^{-1}. This suggests that the through-bond interaction is approximately a factor of 5.1 times larger than the through-space Coulombic interaction. The PME generated anisotropy decay for $V = 2.02$ ns^{-1} ($k = 8.0$ ns^{-1}) is also presented in Figure 8. Though there is a slight decrease in the decay rate compared to the HSR profile, the energy transfer dynamics can be described as predominantly governed by a superexchange tunneling hop from one chromophore to the next. This means that the actual population of excitation onto the bridge is negligible and the McConnell model is thus applicable.

A reference system that can be used to compare with DN-6 is a bichromophore molecule consisting of a naphthalene donor and an anthracene acceptor rigidly separated by a polynorbonane bridge, six σ bonds in length, A-6-N (Figure 1). A measured EET rate of $k = 2.9 \times 10^{10}$ s^{-1} for A-6-N was obtained in this laboratory[34] by exciting the naphthalene chromophore with a picosecond laser and monitoring the time evolution of the emission from the anthracene chromophore. A relationship between the through-bond interaction for the two systems consisting of identical bridges but different chromophores can be obtained from the McConnell's equation.[12] For DN-6 and A-6-N, where only the acceptor molecules are different, we find that

$$\frac{u^{tb}(DN-6)}{u^{tb}(A-6-N)} = \frac{T}{T'} \tag{32}$$

when the approximation of equal energy gaps is made. T/T' is defined as (naphthalene-bridge coupling)/(anthracene-bridge coupling). A rough estimate of T/T' is provided by the ratio of the squares of the sum of the CNDO/S MO coefficients of the

TABLE 1: Fluorescence Decay Data for DN-6 in MTHF at 77 K Monitoring at 334 nm and Recorded at Three Different Excitation Wavelengths λ_{ex}[a]

λ_{ex} (nm)	A	τ (ns)	χ^2	DW
316	42 620	75.56	1.2799	1.9291
317	31 142	73.33	0.9927	2.1249
318	20 159	71.05	1.2535	1.9037

[a] The fluorescence decays were fitted to a monoexponential function, $A \exp(-t/\tau)$, and the goodness of fit was judged by the values of the chi-square value (χ^2) and the Durbin−Watson parameter (DW).

two chromophores at their sites of attachment to the bridge,[12,35,36] i.e.

$$\frac{T}{T'} = \left[\frac{\sum \mathrm{MO(DN-6)}}{\sum \mathrm{MO(A-6-N)}}\right]^2 = \left(\frac{0.512}{0.495}\right)^2. \qquad (33)$$

As the interchromophore orbital-overlap-dependent terms for EET are proportional to the product of two interchromophore molecular orbital overlap integrals, the terms in the above equation are squared.[32,39]

EET in A-6-N is known to occur between the naphthalene's long-axis-polarized ^1L_b state (with substantial borrowing of intensity from the short-axis-polarized ^1L_a state) and both the anthracene's short-axis-polarized ^1L_a state and the long-axis-polarized ^1L_b state.[34] Values of 3.35 and 0.28 cm^{-1} are obtained for u^{tb}(A-6-N) when we consider the short-axis-polarized transition and long-axis-polarized transition, respectively. From eq 35, u^{tb}(DN-6) would therefore lie between 4.8 and 0.4 cm^{-1}. This supports the value of u^{tb}(DN-6) = 1.7 cm^{-1} derived for DN-6, since mixed polarization transitions would occur in A-6-N.[34]

5.2. Inhomogeneous Broadening and its Effects. For the sake of completeness, we report here another possible EET process that may occur in DN-6. Parts a and b of Figure 9 show the emission spectra of DN-6 when excited at different wavelengths within the first absorption band at 77 K and at room temperature, respectively. When the excitation wavelength is increased toward the red-edge of the absorption band, the fluorescence spectrum recorded at 77 K shifts to longer wavelengths, whereas no apparent band shift was observed at room temperature. Furthermore we observe the lifetime of DN-6 at 77 K decreases when the excitation is increased toward the red-edge (see Table 1). This "red-edge" effect[37] indicates the presence of inhomogeneous broadening arising from the existence of multiple energetic sites for the chromophores in the low temperature solvent glass.[38] Directed energy transfer (or dispersive EET) may therefore occur from higher energy naphthalene species to lower energy ones in an inhomogeneously broadened system. We are presently investigating the importance of this effect on the superexchange energy transfer rate.[39]

6. Conclusion

Using the Haken, Strobl, and Reineker stochastic Liouville equations, we have studied the effects of the system−bath interaction on the EET dynamics of a molecular bridged system. Though the HSR model may have some limitations, it still provides adequate information to understand the role of the bridge. It was shown that both the superexchange and sequential mechanisms are operating at the same time but in the limit when the energy gap between the donor and the bridge was very large, as in DN-6, the dominant process is the superexchange mechanism. The energy can tunnel from the donor to the acceptor without actually populating the bridge.

For the case where the energy gap is reduced, the dephasing introduced by the system−bath interaction will increase the importance of the sequential mechanism. This may be relevant for describing energy transfer processes in other multichromophoric arrays such as the aromatic polymer systems described in ref 19. In this case the many intermediate chromophores can play a role in the energy transfer process. When the higher electronic excited states of the intermediate chromophores are far removed from the donor, the superexchange mechanism may contribute. But as discussed in section 4.3, when such polymers are in the condensed phase, bath coupling with those modestly removed higher electronic excited states may trigger the sequential long-range energy transfer process. In this scenario, we may picture the energy hopping as occurring via the higher electronic states of the intermediate molecules before being transferred to the acceptor. A forthcoming paper in this series will explore in greater detail the effects of such higher energy states on the energy transfer kinetics.[40]

Acknowledgment. K.P.G. and M.N.P.R. acknowledge the Australian Research Council for financial support of this work and for the award of a Senior Research Fellowship (to M.N.P.R.). The award of a Melbourne Research Scholarship to E.K.L.Y. is also acknowledged. E.K.L.Y. and K.P.G. are grateful to the ORMOND High-Performance Computing facility for the use of the Cray J916 computer.

References and Notes

(1) *J. Phys. Chem. B* **1997**, *101*, 7197−7359 consists of a collection of papers that were presented at the *Light-Harvesting Physics Workshop*, Bristonas, Lithuania, 14−17 September 1996.
(2) Hu, X.; Schulten, K. *Phys. Today* **1997**, *50*, 28.
(3) Guillet, J. *Polymer Photophysics and Photochemistry*; Cambridge University Press: London, 1985.
(4) Ghiggino, K. P.; Smith, T. A. *Prog. Reaction Kinet.* **1993**, *18*, 375.
(5) Van Der Meer, W. B.; Coker, G.; Chen, S. S−Y. *Resonance Energy Transfer*; VCH Publishers: New York, 1994.
(6) Sienicki, K. *J. Chem Phys*. **1991**, *94*, 617.
(7) Förster, Th. In *Modern Quantum Chemistry*; Sinanoglu, O., Ed.; Academic Press: New York, 1965; p 93.
(8) Harcourt, R. D.; Scholes, G. D.; Ghiggino, K. P. *J. Chem. Phys*. **1994**, *101*, 10521.
(9) Scholes, G. D.; Harcourt, R. D.; Ghiggino, K. P. *J. Chem. Phys*. **1995**, *102*, 9574.
(10) Scholes, G. D. *J. Phys. Chem*. **1996**, *100*, 18731.
(11) Scholes, G. D.; Ghiggino, K. P. In *Advances in Multiphoton Processes and Spectroscopy*, *Vol 10*; Lin, S. H., Villaeys, A. A., Fujimura, Y., Eds.; World Scientific: Singapore, 1996; p 95.
(12) Jordan, K. D.; Paddon-Row: M. N. *Chem. Rev*. **1992**, *92*, 395.
(13) McConnell, H. M. *J. Chem. Phys*. **1961**, *35*, 508.
(14) Guo, H.; Liu, L.; Lao, K,-q. *Chem. Phys. Lett.* **1994**, *218*, 212.
(15) Sumi, H.; Kakitani, T. *Chem. Phys. Lett*. **1996**, *252*, 85.
(16) Okada, A.; Chernyak, V.; Mukamel, S. *J. Phys. Chem. A* **1998**, *102*, 1241.
(17) Felts, A. K.; Pollard, W. T.; Friesner, R. A. *J. Phys. Chem*. **1995**, *99*, 2929.
(18) Davis, W. B.; Wasielewski, M. R.; Ratner, M. A.; Mujica, V.; Nitzan, A. *J. Phys. Chem. A* **1997**, *101*, 6158.
(19) Ghiggino, K. P.; Yeow, E. K. L.; Haines, D. J.; Scholes, G. D.; Smith, T. A. *J. Photochem. Photobiol. A: Chem*. **1996**, *102*, 81.
(20) Scholes, G. D.; Ghiggino, K. P.; Oliver, A. M.; Paddon-Row, M. N. *J. Am. Chem. Soc.* **1993**, *115*, 4345.
(21) Haken, H.; Strobl, G. *Z. Phys*. **1973**, *262*, 135.
(22) Haken, H.; Reineker, P. *Z. Phys*. **1972**, *249*, 253.
(23) Reineker, P. In *Exciton Dynamics in Molecular Crystals and Aggregates*; Springer: Berlin, 1982. See also the article by Kenkre, V. M. in this book.
(24) Leegwater, J. A. *J. Phys. Chem*. **1996**, *100*, 14403.
(25) Szocs, V.; Banacky, P. *Chem. Phys.* **1994**, *186*, 161.
(26) Paddon-Row, M. N.; Patney, H. K. *Synthesis* **1986**, 328.
(27) Phillips, D.; O'Connor, D. V. *Time-Correlated Single Photon Counting*; Academic Press: New York, 1983.

(28) Blum, K. *Density Matrix Theory and Applications*, 2nd ed.; Plenum Press: New York, 1996.

(29) Rahman, T. S.; Knox, R. S.; Kenkre, V. M. *Chem. Phys.* **1979**, *44*, 197.

(30) Smith, B. T.; Boyle, J. M.; Dongarra, J. J.; Moler, B. B. In *Lecture Notes in Computer Science, Vol 6: Matrix Eigensystem Routines—EISPACK Guide*; Goos, G., Hartmanis, J., Eds.; Springer-Verlag: New York, 1976.

(31) Dongarra, J. J.; Moler, C. B.; Bunch, J. R.; Stewart, G. W. *LINPACK User's Guide*; SIAM: Philadelphia, 1992.

(32) Clayton, A. H. A.; Scholes, G. D.; Ghiggino, K. P.; Paddon-Row, M. N. *J. Phys. Chem*. **1996**, *100*, 10912.

(33) Eriksson, S.; Källebring, B.; Larsson, S.; Martensson, J.; Wennerström, O. *Chem. Phys.* **1990**, *146*, 165.

(34) Scholes, G. D.; Ghiggino, K. P.; Oliver, A. M.; Paddon-Row, M. N. *J. Phys. Chem.* **1993**, *97*, 11871.

(35) Paddon-Row, M. N.; Patney, H. K.; Peel, J. B.; Willett, J. D. *J. Chem. Soc., Chem. Commun.* **1984**, 564.

(36) Balaji, V.; Ng, L.; Jordan, K. D.; Paddon-Row, M. N.; Patney, H. K. *J. Am. Chem. Soc.* **1987**, *109*, 6957.

(37) Weber, G. *Biochem. J*. **1960**, *75*, 335.

(38) Demchenko, A. P. *Ultraviolet Spectroscopy of Proteins*; Springer-Verlag: Berlin, 1986.

(39) Yeow, E. K. L.; Ghiggino, K. P. Unpublished work.

(40) Yeow, E. K. L.; Ghiggino, K. P. Unpublished work.